DOI: 10.13009/EUCASS2019-702

DOI: ADD DOINUMBER HERE

Design of a Model-Based Failure Detection Isolation and Recovery System for Cubesats

Javier Sanz Lobo[⋆]*, Pablo Ghiglino* [⋆⋆]*, Said López Escobedo* [⋆⋆⋆] *and Manuel Sanjurjo Rivo*[⋆†]
[⋆]*Bioengineering and Aerospace Engineering Department, Universidad Carlos III de Madrid*
Avenida de la Universidad 30, 28911, Leganes (Madrid), Spain
[⋆⋆] *Klepsydra Robotics*
[⋆⋆⋆] *Instituto Nacional de Astrofísica, Óptica y Electrónica*
San Andrés Cholula (México)
javier.s.lobo@alumnos.uc3m.es · pablo.ghiglino@klepsydra.org · mat.cobaev@gmail.com · msanjurj@ing.uc3m.es
[†]Corresponding author

Abstract

The number of CubeSats launched has exponentially grown in recent years owing to being a competitive solution for space applications. The present study is focused on increasing its lifetime, safety and autonomy level. A cost-effective way to achieve it is designing an active fault-tolerant control system (AFTCS) to detect, isolate and accommodate faults affecting the CubeSat. More precisely, the techniques proposed are implemented on the Attitude and Orbit Control System (AOCS), one of the most safety-critical subsystems. They are tested in a Matlab & Simulink® environment demonstrating their extraordinary potential and enormous advantages.

1. Introduction

CubeSats are recognized as a competitive solution for space missions since they provide an excellent equilibrium between development time, cost, lifetime and replacement, which are crucial to guarantee the success of the project. This, together with the rising advances in miniaturization of components have exponentially increased the number of CubeSats launched in recent years.

Despite the growing interest and investment in CubeSats projects, they are far from offering the level of reliability of conventional satellites. Accordingly, the design of a Failure Detection, Isolation and Recovery (FDIR) system is highly advantageous in terms of ensuring safety and increasing the autonomy level of the CubeSat. FDIR has an important impact on the safety, mass, cost, performance and ultimately reliability of a space system, in particular for the AOCS subsystem in autonomous spacecraft and space vehicles. The current practice in space missions is to achieve FDIR through physical redundancy, while newer approaches propose alternative solutions such as model-based FDIR techniques (analytical redundancy), to be implemented in a complementary manner or in place of redundancy. Model-based techniques intend to supplement physical redundancy, allowing to reach higher reliability levels in the system, without the necessity of additional hardware. However, the computation capabilities of CubeSats are extremely limited and, therefore, an efficient implementation of the FDIR system is mandatory.

This work aims to trade-off hardware and analytical redundancy in the specific case of a CubeSat mission using state-of-the-art model-based techniques and Klepsydra, a high performance and lightweight software development toolset for space embedded systems. This product can process large amount of data in real time while simultaneously optimises the computational resources. The objective is to test the results in an actual CubeSat mission application. In the present paper, the focus is on the implementation of a FDIR system on an Earth observation satellite and, particularly, on the Attitude and Orbital Control System (AOCS), one of the most FDIR sensitive subsystem. Nevertheless, the methodology can be potentially extended to any CubeSat mission and any subsystem. In the frame of Earth observation missions, the objective is to reduce the dependency on ground commands and have on-board capability of solving the most common failures. The AOCS is responsible for maintaining the satellite in its orbit and the pointing accuracy inside the required range. Therefore, the accommodation of the faults affecting the actuators and sensor of the AOCS is critical for the safety completion of the mission.

DOI: 10.13009/EUCASS2019-702

The FDIR techniques proposed in this paper were tested in a simulation environment and satellite subsystems previously modelled in Matlab & Simulink®. The use of block diagrams allows faster development, better visualization, integration with external hardware and more flexibility. Additionally, it provides the tools to code stochastic hybrid systems, where continuous dynamics -environment-, discrete dynamics -actuators, sensors and controllers with different update rates- and probabilistic uncertainty- actuators, sensor and model errors- interact.

The paper is organized as follows: the first section briefly describes the mission, the CubeSat model and its AOCS. Then, the theoretical basements of the FDIR techniques and the results of their performances are presented. Finally, some concluding remarks are given.

2. Mission baseline

The aim of this section is to describe the model mission, the main parameters of the CubeSat design and the AOCS configuration. Design of FDIR system should be tailored to a specific mission and platform, but the methodology presented in this paper can be extended to any mission.

2.1 Orbit overview

CubeSats are generally placed in Low Earth orbits because it guarantees optimum conditions for telecommunications and protection for solar and cosmic radiation. In this paper, it was proposed a standard Earth observation mission with an optical payload permanently pointed to Nadir, which toughens the AOCS requirements and hence, the FDIR ones.

Sun-synchronous orbits (SSO) were considered the most propitious orbit for the mission. This choice was based on the global coverage provided at all latitudes due to its nearly polar inclination. In addition, it offers a constant lightning and thermal conditions by using the J2 perturbation to maintain the position of the line of nodes fixed with respect to the sun's direction. As a first approach, a noon-midnight orbit was chosen to minimize the shadows in the dayside (see Table 1).

Table 1: Characteristics of the SSO selected

Parameter	Value	Unit
Semimajor axis	6795	km
Eccentricity	0	n/a
Inclination	97.1	deg
Type	12h-24h	n/a

2.2 CubeSat configuration

The satellite selected to perform the previously described mission was a 2U CubeSat. Therefore, its size is 10x20x10 cm, and it weighs 2.66 kg. Figure 1 illustrates the relative position of the external elements with respect to the body axis, the Earth and the orbit motion. The propulsion system was placed in the opposite face to the orbit motion to counteract the drag, which is the responsible for orbit decay, and the optical payload pointing to Nadir.

The Figure 2 offers a general view of the interaction between the different components that participate in the 6 degree-of-freedom (DOF) control of the CubeSat. The AOCS compares the measurements provided by the sensors with the desired path given by the guidance block to compute the forces and moments needed to follow the guidance commands.

The control relies on the following sensors: a GPS receiver to provide the position $\mathbf{r}$, the speed $\mathbf{v}$ and timing information for computational operations; a set of gyroscopes in hot redundancy to measure the angular rate of the satellite $\mathbf{w}$; and a star tracker to accurately determine the attitude quaternion $\mathbf{q}$.

These sensors are subjected to uncertainties due to noise and bias, which were modelled as independent zero-mean Gauss noise processes whose standard deviations were selected from data of CubeSat components manufacturers.

The mission of the navigation unit is to achieve reliable estimations $\hat{\boldsymbol{r}}$, $\hat{\boldsymbol{v}}$, $\hat{\boldsymbol{w}}$ and $\hat{\boldsymbol{q}}$ of the measurements reducing the commented noise. For orbit determination, it was followed the methodology described by [4] to design a simple

DOI: 10.13009/EUCASS2019-702

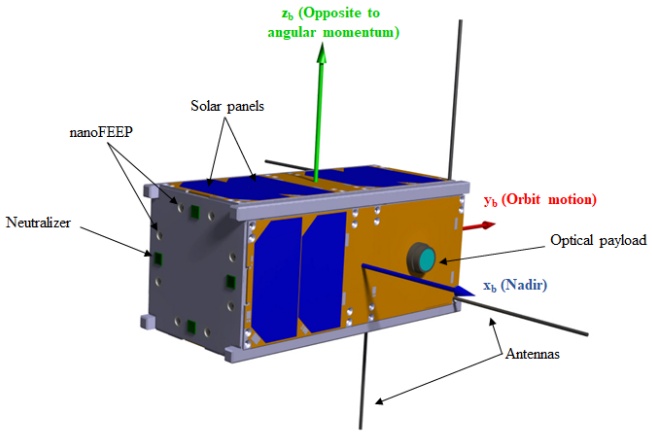

Figure 1: 3D representation of the 2U CubeSat employed in the mission

Kalman Filter for the GPS signal. The case of the attitude determination is more complex: the use of two different sensors for attitude measurements demands the implementation of an algorithm that combines both to obtain a better estimation than considering each sensor separately. Therefore, it was designed a Multiplicative Quaternion Extended Kalman Filter (MQEKF) that allows to accurately determine the attitude when the star tracker is not available and actualize the information of the gyroscopes to correct the integration error [3].

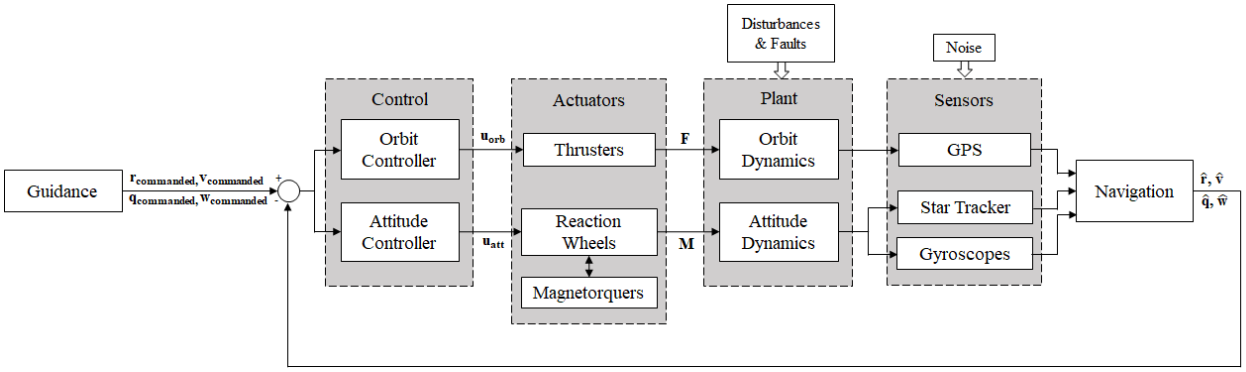

Figure 2: GNC system scheme

As shown in figure above, the 6 DOF control was subdivided in two controllers: one dedicated to the orbit maintenance and the other dedicated to nadir pointing. The control system logic was based on a standard Linear Quadratic Regulator (LQR) in both cases. The LQR uses the state feedback estimations to find the optimal control, which consists of a trade-off between regulation performances and control effort. Although it cannot be used in non-linear systems, it is perfect for the problem analysed: simple, accurate, very little memory requirement and suited for multiple-input/multiple-output systems (MIMO) with small deviations around the equilibrium [10]. It is important to remark that the AOCS and the FDIR system were designed for the nominal mode of the satellite after detumbling.

For the autonomous orbit control, it was used a virtual formation model in which the satellite affected by the perturbations (chaser) tries to follow a virtual reference affected only by the Earth's gravity (target). This motion is expressed in terms of relative orbital elements, and the Gauss' variational equations for near-circular non-equatorial orbits are linearised to apply the LQR [2]. The control effort was focused on maintaining the height of the orbit to avoid the decay due to drag, and the inclination, which is essential to preserve the correct orbital precession. Finally, a signal is sent to a redundant set of 8 highly miniaturized Field Emission Electric Propulsion thrusters (nanoFEEP), which are able to provide continuous thrust at μN levels in an efficient way [1]. As shown in Figure 3, the orbit controller perfectly works without system faults, and the controlled altitude converges to the nominal one instead of rapidly decay.

For the attitude control, the CubeSat relies on a quaternion feedback control to generate the commands sent to a redundant set of 4 reaction wheels [9]. However, their final saturation due to the secular component of perturbations requires a way to exert an external torque. The magnetorquers are in charge of creating a magnetic torque to compensate

DOI: 10.13009/EUCASS2019-702

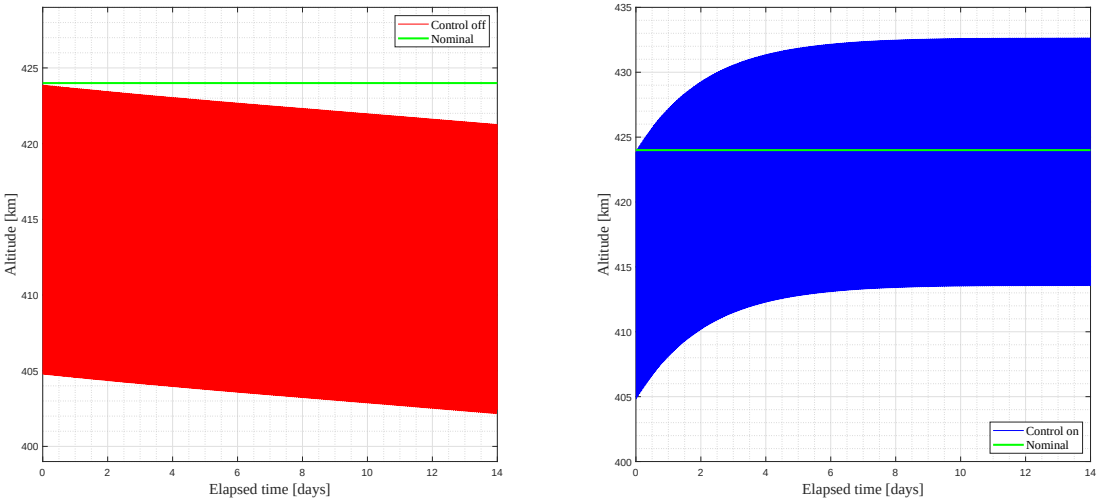

(a) Control off

(b) Control on

Figure 3: Orbit controller validation

it following a low-level control law, which desaturates the reaction wheels without altering the principal attitude control [6]. Before designing the FDIR system, the proper operation of the controller was tested and validated (see Figure 4). The Euler angles shown are the ones defined between the body axis presented in Figure 1 and the local-vertical local-horizontal (LVLH) frame, so that the Euler angles for perfect pointing are respectively 90^o, 0^o and 90^o.

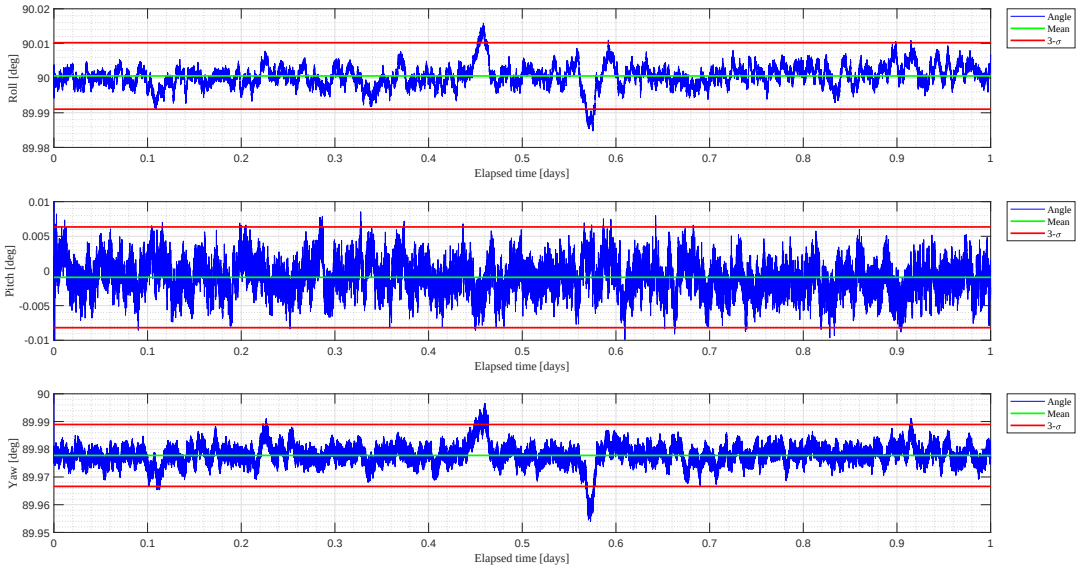

Figure 4: Attitude controller validation

3. FDIR design

The AOCS described in the previous section is fundamental to achieve the mission objectives and fulfil the pointing requirement. However, to guarantee the mission success, the CubeSat has to be equipped by an AFTCS that actively reacts to system faults by controller re-design to ensure stability and maintenance of the system performances.

DOI: 10.13009/EUCASS2019-702

The AFTCS tasks can be condensed in three. The first task is the fault detection, which indicates the occurrence of a fault in the monitored system. The second task is the fault isolation which consists of detecting the type and/or location of the fault. Finally, the fault recovery is in charge of the accommodation through controller redesign [5]. In the present paper, the AFTCS was focused on the most faulty components of the AOCS according to an extensive study based on 129 military and commercial spacecrafts from 1980 to 2005 (see Figure 5): thruster (24%), gyroscope (17%) and wheel (16%). Therefore, it was achieved to cover more than 50% of the faults.

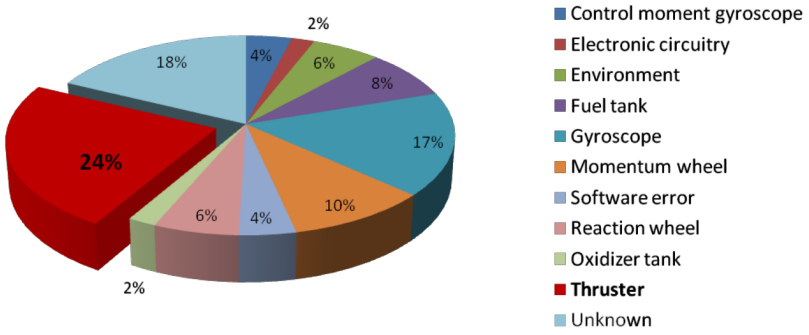

Figure 5: Distribution of AOCS component faults [5]

The fault detection on these components is divided in there hierarchical levels:

- The Level 1 consists of individually monitoring the output of all the gyroscopes to detect sudden sensor death and frozen signal fault types.
- The Level 2 checks consistency between the measurements of gyroscopes to determine faults not seen by Level 1, such as slow drift.
- Once the sensor faults are discarded, the Level 3 looks for inconsistencies between the sensors and commands sent to the actuators.

3.1 Gyroscope

The Inertial Navigation System (INS) is composed of 6 single-axis MEMS gyroscopes, which are grouped in two Inertia Management Units (IMU) to create a dedicated pyramid configuration (see Figure 6). The use of this set ensures the reliability and accuracy of navigation minimizing the number of redundant hardware.

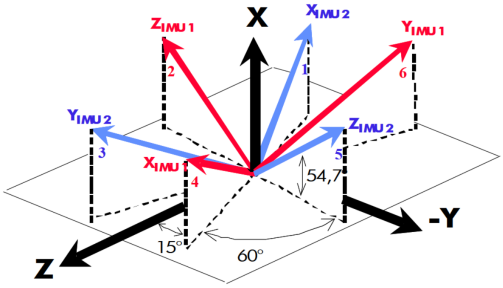

Figure 6: Gyroscopes configuration [5]

The angular rate of the satellite **w** is obtained by the least square method through the left Moore-Penrose inverse of the gyroscopes configuration matrix:

$$\boldsymbol{w} = \left(\boldsymbol{H}^T \boldsymbol{H}\right)^{-1} \boldsymbol{H}^T \boldsymbol{m} \tag{1}$$

where $\mathbf{H} \in \mathbb{R}^{6x3}$ is the configuration matrix and **m** is the column vector of the measurements from gyroscopes. If a faulty gyroscope is detected, it is switched off and its corresponding row in **H** is deleted.

DOI: 10.13009/EUCASS2019-702

Following the hierarchy previously presented, the first task of the AFTCS is to detect and isolate the sudden death and frozen signal events. To detect a sudden death, the derivative of the output of each gyroscope is monitored. If a signal becomes null after an abrupt change in the derivative, which means the presence of a big discontinuity, an alarm of "death sensor" is immediately activated and the related gyroscope is switch off.

In case of lock-in-place gyroscope, its standard deviation is calculated online through a fixed sliding window $N_d \in \mathbb{Z}^+$. When a gyroscope is healthy, the standard deviation of its measurement is higher than the one given by the manufacturer, even in the case of constant angular rate commanded, due to the small error introduced by the attitude controller. However, the standard deviation will be nearly the one given by the manufacturer if the signal is frozen because the noise of the gyroscope is the only responsible of the variation from the constant value (see Figure 7).

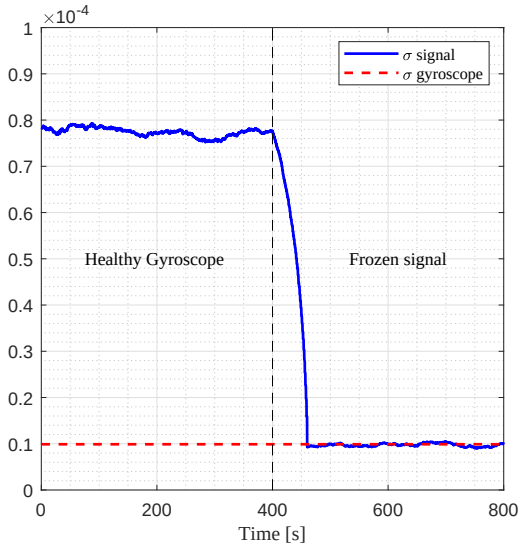

Figure 7: Analysis of the standard deviation of gyroscope signal

The pyramid dedicated configuration provides the equations needed to perform the consistency check in Level 2. A set of 9 residuals are generated through static parity space approach, which have a zero-mean value in case of fault-free condition [8]. These residual were evaluated by a Generalized Likelihood Ration (GLR) test to detect changes in the mean [5]. If the GLR test is higher than a given threshold, a Boolean is set, and the faulty gyroscope is detected and isolated following the logic explained below.

The failure detection is based on three residuals:

$$r_1 = (m_1 + m_4) - (m_2 + m_5) \tag{2}$$

$$r_2 = (m_2 + m_5) - (m_3 + m_6) \tag{3}$$

$$r_3 = (m_3 + m_6) - (m_1 + m_4) \tag{4}$$

where r_i (i = 1,...,3) is the set of residual used for detection and m_j (j = 1,...,6) is the measurement of the j^{th} gyroscope.

As shown in Table 2, there are 5 cases in which it is not possible to determine the valid conclusion. For the isolation phase, the remaining residuals are employed:

$$r_4 = 2\,(m_1 + m_3 + m_5) - 3\,(m_1 + m_4) \tag{5}$$

$$r_5 = 2\,(m_2 + m_4 + m_6) - 3\,(m_1 + m_4) \tag{6}$$

$$r_6 = 2\,(m_1 + m_3 + m_5) - 3\,(m_2 + m_5) \tag{7}$$

$$r_7 = 2\,(m_2 + m_4 + m_6) - 3\,(m_2 + m_5) \tag{8}$$

$$r_8 = 2\,(m_1 + m_3 + m_5) - 3\,(m_3 + m_6) \tag{9}$$

DOI: 10.13009/EUCASS2019-702

Table 2: Fault Detection Table

First tests for fault detection				
$r_1 < TH_1$	$r_2 < TH_2$	$r_3 < TH_3$	Conclusion	
True	False		Fault on Gyro #6 Fault on Gyro #3 and #6 Fault on Gyro #3	**1**
	True		More than two faulty gyros	**2**
False	False	True	Fault on Gyro #2 Fault on Gyro #2 and #5 Fault on Gyro #5	**3**
		False	Two or more faulty gyros	**4**
	True		Fault on Gyro #4 Fault on Gyro #1 and #4 Fault on Gyro #1	**5**

$$r_9 = 2\,(m_2 + m_4 + m_6) - 3\,(m_3 + m_6) \tag{10}$$

where r_i (i = 4,...,9) is the set of residual used for isolation.

Table 3: Fault Isolation Table

	Second tests for fault isolation						
	$r_4 < TH_4$	$r_5 < TH_5$	$r_6 < TH_6$	$r_7 < TH_7$	$r_8 < TH_8$	$r_9 < TH_9$	Conclusion
1	True						Fault on Gyro #6
	False	False					Fault on Gyro #3 and #6
		True					Fault on Gyro #3
2							More than two faulty gyros
3	True						Fault on Gyro #2
	False	False					Fault on Gyro #2 and #5
		True					Fault on Gyro #5
4	True						Fault on Gyro #2 and #6
		True					Fault on Gyro #3 and #5
			True				Fault on Gyro #4 and #6
				True			Fault on Gyro #1 and #3
					True		Fault on Gyro #2 and #4
						True	Fault on Gyro #1 and #5
							Two or more faulty gyros
5			True				Fault on Gyro #4
			False	False			Fault on Gyro #1 and #4
				True			Fault on Gyro #1

Figure 8 and 9 show the reader how these methodology works. After introducing a drift in gyroscope #1 at time t = 500 s, some residuals start growing and their mean value becomes non-zero. If the reader applies the logic summarized in the previous tables to the residuals of Figure 9, they can detect and isolate the faulty gyroscope.

The FDIR techniques proposed for gyroscopes are simple, fast, and require very little memory and hardware redundancy. On the other hand, the space parity approach must be complemented by other technique to be able to cover all possible faults, i.e., more than two faulty gyroscopes.

3.2 Reaction wheel

Reaction wheels are angular momentum exchange devices in charge of the primary attitude control. They respond to disturbances on the the CubeSat by changing the angular rate of the wheel from its nominal value in order to preserve the desirable attitude with high accuracy. Therefore, any undetected fault would make impossible to continue pointing to nadir.

DOI: 10.13009/EUCASS2019-702

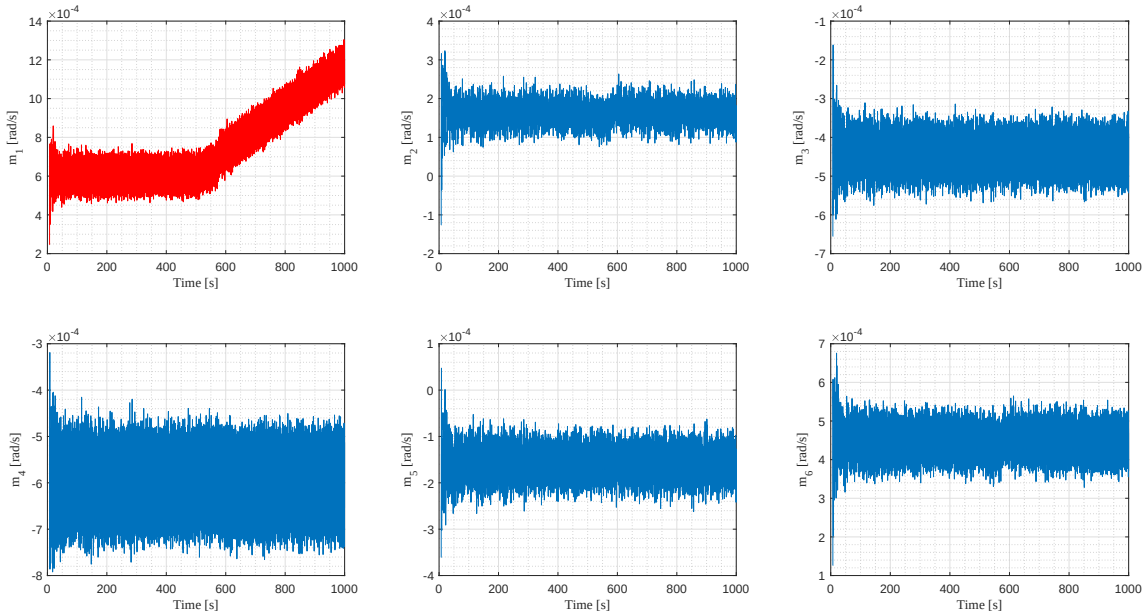

Figure 8: Measurements of gyroscopes with drift in m_1

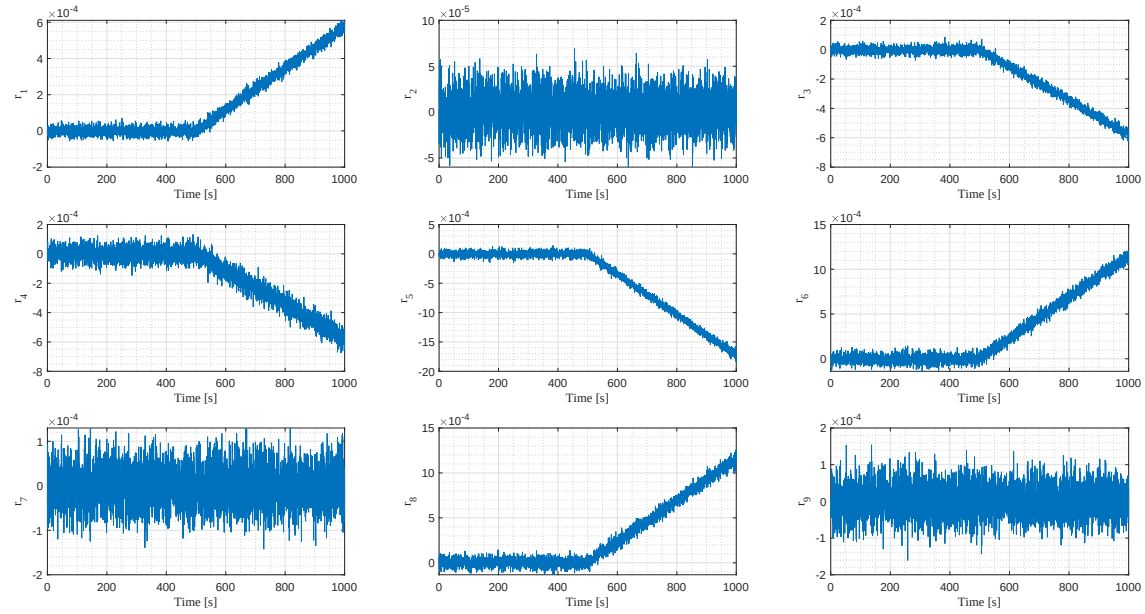

Figure 9: Evolution of residuals of Level 2 in a faulty event

To obtain a fault tolerant system, the present paper proposed a redundant set of 4 reaction wheels in a pyramid configuration with z_b axis as the main one since the attitude control demands the highest moment in this axis (see Figure 10). It is clear that this configuration can only deal with one faulty reaction wheel because two faulty reaction wheels lead to an unfeasible allocation problem, i.e., distributing the three components of the moment vector between two wheels.

The wheel/tachometer consistency checks are in Level 3 where it was assumed that sensor faults have been detected and isolated, so that the measurements are reliable. Each wheel was equipped with a tachometer that measures

DOI: 10.13009/EUCASS2019-702

its angular rate w_{rw}, which was used to elaborate the residual r_{rw} to determine the fault existence through the equation of its working principle:

$$T_{rw}(t) = -\dot{h}_{rw} = -\frac{d(I_{rw}w_{rw})}{dt} = -I_{rw}\frac{dw_{rw}}{dt} \tag{11}$$

$$r_{rw} = T_{rw}(t) - T_c(t) \tag{12}$$

where I_{rw} is the inertia of the wheel, h_{rw} is the angular momentum of the wheel, T_{rw} is the actual torque of the wheel and T_c is the torque commanded by the attitude controller. For decision making, it was applied a simple threshold-based approach to the moving root-mean-square (RMS) of the residual, and the accommodation consists of eliminate the faulty wheel from the configuration matrix and redesign the gain matrix of the LQR control law.

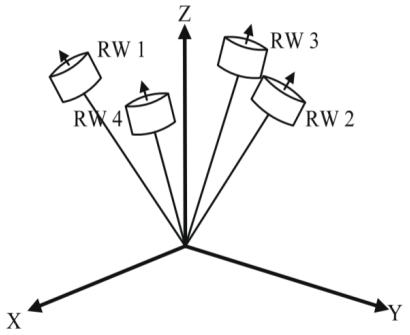

Figure 10: Reaction wheels configuration [7]

3.3 Thruster

The propulsion subsystem of the CubeSat consists of 8 nanoFEEP whose main task is to compensate the orbit decay due to the atmospheric drag and maintain the nominal inclination. They provide continuous thrust by applying a high potential between a needle wetted with liquid metal (e.g. gallium or indium) and electrode. The liquid metal of the tip of the needle is evaporated and ionized and ,finally, the ions are accelerated due to the applied electric field delivering the thrust. Figure 11 shows how the thrusters were arranged in the face opposite to motion of the satellite.

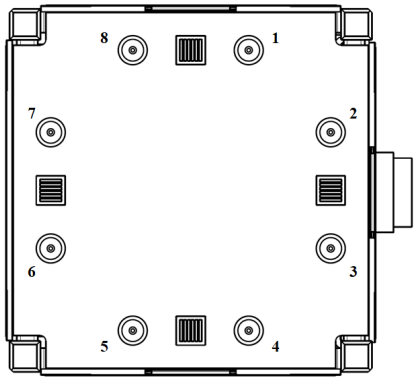

Figure 11: Thrusters configuration

Following the FDIR technique applied to reaction wheels, one can think about placing several sensors in each thruster to measure representative variables, such as temperature. However, this implies extra cost, mass and complexity. Alternatively, it is proposed a model-based FDIR approach that uses the available on-board input-output relations.

3.3.1 Residual generator

The residual generator was based on the target pointing mode of the attitude control system, whose dynamics can be expressed by the Euler's rotational equation:

DOI: 10.13009/EUCASS2019-702

$$\dot{\boldsymbol{w}}(t) = \boldsymbol{I}_{sc}^{-1}\left[\boldsymbol{d}(t) + \boldsymbol{T}_{prop}(t) + \boldsymbol{T}_{rw}(t) + \boldsymbol{T}_{mt}(t)\right] - \boldsymbol{I}_{sc}^{-1}\left[\boldsymbol{w}(t) \times \boldsymbol{I}_{sc} \cdot \boldsymbol{w}(t) + \boldsymbol{h}_{rw}(t)\right] \tag{13}$$

where $\boldsymbol{I}_{sc} \in \mathbb{R}^{3x3}$ is the spacecraft tensor of inertia, $\boldsymbol{d}$ is the disturbance torque (gravity gradient, magnetic, aerodynamic and noise), $\boldsymbol{T}_{prop}$, $\boldsymbol{T}_{rw}$ and $\boldsymbol{T}_{mt}$ is respectively the torque exerted by thrusters, reaction wheels and magnetorquers.

Considering that the thrusters only exert torque in faulty situations and the effects of wheels and magnetorquers can be grouped in a unique control vector $\boldsymbol{u}_{att}$, the previous equations is rearranged as:

$$\dot{\boldsymbol{w}}(t) = \boldsymbol{I}_{sc}^{-1}\left[\boldsymbol{d}(t) + \boldsymbol{f}(t) + \boldsymbol{u}_{att}(t)\right] - \boldsymbol{I}_{sc}^{-1}\left[\boldsymbol{w}(t) \times \boldsymbol{I}_{sc} \cdot \boldsymbol{w}(t)\right] \tag{14}$$

where $\boldsymbol{f}$ is the fault vector.

Since the CubeSat is controlled around the equilibrium point $\boldsymbol{w}_n = [0, 0, -\left(\mu/a^3\right)^{1/2}]^T$, it is possible to linearize the model by means of a first-order approximation of the previous non-linear equation:

$$\begin{cases} \dot{\boldsymbol{x}}(t) = \boldsymbol{A}\boldsymbol{x}(t) + \boldsymbol{B}\boldsymbol{u}_{att}(t) + \boldsymbol{E}_f\boldsymbol{f}(t) + \boldsymbol{E}_d\boldsymbol{d}(t) \\ \boldsymbol{y}(t) = \boldsymbol{C}\boldsymbol{x}(t) \end{cases} \tag{15}$$

$$\boldsymbol{A} = \left(-\boldsymbol{I}_{sc}^{-1}\frac{\partial(\boldsymbol{w} \times \boldsymbol{I}_{sc})}{\partial \boldsymbol{w}}\right)_{|w_n}, \quad \boldsymbol{B} = \boldsymbol{E}_f = \boldsymbol{E}_d = \boldsymbol{I}_{sc}^{-1}, \quad \boldsymbol{C} = \begin{bmatrix} 1 & 0 & 0 \\ 0 & 1 & 0 \\ 0 & 0 & 1 \end{bmatrix} \tag{16}$$

where $\boldsymbol{x}$ and $\boldsymbol{y}$ is respectively state and measurement vector.

Once the linear time-invariant (LTI) system is defined, it is applied an estimation technique to it. The aim is to detect unusual changes in the system behavior by monitoring the difference between the real measurements and the estimated output vector (see Figure 12).

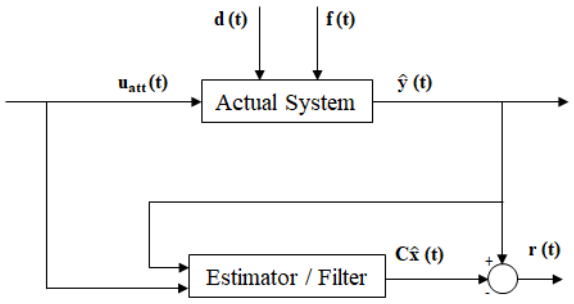

Figure 12: Scheme of the residual generator

To solve the estimation problem, it was selected the Kalman filter. Before applying it to the described system, it has to be discretised according to the sampling frequency T_s in which gyroscopes provide measurements of the state vector.

$$\begin{cases} \boldsymbol{x}(k+1) = \boldsymbol{A}_d\boldsymbol{x}(k) + \boldsymbol{B}_d\boldsymbol{u}_{att}(k) + \boldsymbol{E}_{fd}\boldsymbol{f}(k) + \boldsymbol{E}_{dd}\boldsymbol{d}(k) \\ \boldsymbol{y}(k) = \boldsymbol{C}_d\boldsymbol{x}(k) \end{cases} \tag{17}$$

$$\boldsymbol{A}_d = e^{AT_s} \simeq I_{3x3} + T_s\boldsymbol{A}, \quad \boldsymbol{B}_d = \boldsymbol{E}_{fd} = \boldsymbol{E}_{dd} = \int_0^{T_s} e^{A\tau}d\tau\boldsymbol{B} \simeq T_s\boldsymbol{B}, \quad \boldsymbol{C}_d = \boldsymbol{C} \tag{18}$$

The Kalman filter finds an optimal estimate (minimum mean squared error) of the state of an uncertain and linear system. It has two steps: prediction, in which the state of the system is firstly predicted forward in time using the dynamic model of the system, and correction, in which the previous prediction is corrected using the information known from the measurement [8].

DOI: 10.13009/EUCASS2019-702

Prediction step:

$$\hat{\boldsymbol{x}}_k^- = \boldsymbol{A}_d \hat{\boldsymbol{x}}_{k-1} + \boldsymbol{B}_d \boldsymbol{u}_{attk} \tag{19}$$

$$\boldsymbol{P}_k^- = \boldsymbol{A}_d \boldsymbol{P}_{k-1}^- \boldsymbol{A}_d^T + \boldsymbol{Q}_k \tag{20}$$

Correction step:

$$\boldsymbol{K}_k = \boldsymbol{P}_k^- \boldsymbol{C}_d^T \left(\boldsymbol{C}_d \boldsymbol{P}_k^- \boldsymbol{C}_d^T + \boldsymbol{R}_k \right)^{-1} \tag{21}$$

$$\hat{\boldsymbol{x}}_k = \hat{\boldsymbol{x}}_k^- + \boldsymbol{K}_k \left(\hat{\boldsymbol{y}}_k - \boldsymbol{C}_d \hat{\boldsymbol{x}}_k^- \right) \tag{22}$$

$$\boldsymbol{P}_k = (I_{3x3} - \boldsymbol{K}_k \boldsymbol{C}_d) \boldsymbol{P}_k^- \tag{23}$$

Residual:

$$\boldsymbol{r}_k = (\hat{\boldsymbol{y}}_k - \boldsymbol{C}_d \hat{\boldsymbol{x}}_k) \tag{24}$$

where $\hat{\boldsymbol{x}}$ is the estimation of the state vector, $\boldsymbol{K}_k$ is the Kalman gain that tries to minimize the estimation error, $\boldsymbol{P}_k$ is the state vector covariance matrix, $\hat{\boldsymbol{y}}$ is the estimation of the angular rate given by the Navigation unit, $\boldsymbol{R}$ is the covariance matrix of $\hat{\boldsymbol{y}}$ obtained from the MQEKF and $\boldsymbol{Q}$ is the covariance matrix of the process noise.

Faults, spatial disturbances and noise due to uncertainties (e.g. thrust misalignment or variation of the mass properties of the CubeSat) are responsible for taking the residual away from zero-mean value. However, the filter is tuned to be only sensitive to the torque due to faulty thrusters, which is one or two order of magnitude larger than the remaining effects.

3.3.2 Fault detection and isolation

The considered faults to be detected and isolated are nanoFEEP blocking itself during operation (mechanical fault) and closing itself (electronic fault) [11], so that the force exerted becomes null instead of being the commanded one. Assuming no simultaneous faults, the satellite experiments a torque opposite to the one compensated by the faulty thruster. In this situation, the attitude controller has to make an extra effort that is reflected in the three components of the residual.

Each thruster generates eight different moments (see Table 4). Therefore, the faulty thruster can be detected and isolated by monitoring the tendency of the moving average through a fixed sliding window $N_d \in \mathbb{Z}^+$.

Table 4: Sign of the torque components of each thruster

Thruster Number	T_x	T_y	T_z
1	-	+	+
2	-	-	+
3	+	+	+
4	+	-	+
5	+	+	-
6	+	-	-
7	-	+	-
8	-	-	-

Finally, the fault is accommodated by modifying the configuration matrix used in the control allocation problem and adapting the gain of the LQR control law. The tests showed that the configuration proposed is able to continue correcting the orbit with N-1 thrusters. On the other hand, when the number of faulty thrusters is larger, the allocation strategy has difficulties to find a feasible solution due to the constraint of not exerting external torque given to the propulsion system and the fact that the thrust is unidirectional. In this case, the option of simultaneously correcting inclination and altitude would not be available.

To illustrate how this model works, it is analysed the situation in which thruster #7 fails. Looking at Fig. 13, the mean of the three components of the residual remains near zero and, thus, the GLR test of each one is below the threshold. However, they rapidly change when a fault is introduced at t = 1350 s.

DOI: 10.13009/EUCASS2019-702

When one of the threshold is surpassed, the algorithm immediately determines the faulty thruster by monitoring the tendency of the mean value of the residuals. In this case, the thruster #7 is isolated because this tendency is opposite to the torque exerted by this thruster (see Table 4). Once the accommodation happens, the residuals and corresponding GLR test recover their normal value.

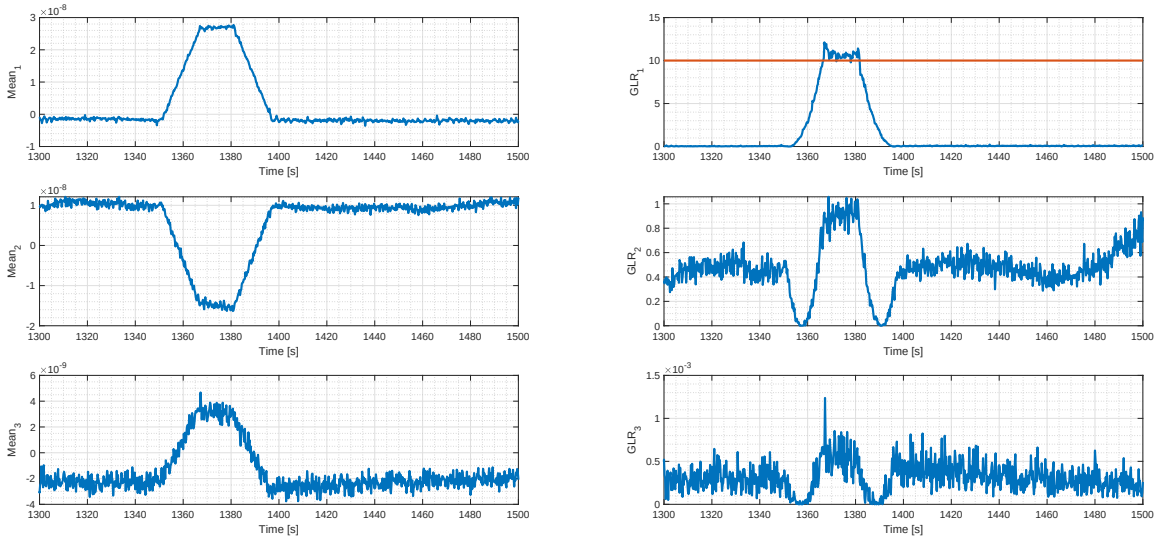

(a) Evolution of the mean value

(b) Evolution of the GLR test

Figure 13: Results of monitoring a fault in thruster #7

4. Conclusion

Design and implementation of three model-based FDIR techniques for the AOCS of a CubeSat in an Earth observation mission has been presented. They have been the result of an exhaustive analysis of the current state-of-art of FDIR systems in the space segment. The most complicated part was adapting the acquired knowledge to the special characteristics of CubeSat: low-cost, tiny size, and power and mass budget constraints. To fulfil these requirements, it was proposed the use of the available information on-board and minimization of the redundant components needed.

In this context, the paper was focused on firstly developing a FDIR system that was able to deal with the faultiest and most safety-critical components of the AOCS -gyroscope, reaction wheel and thruster- and then, testing it in a Matlab & Simulink® environment. Although the results confirmed its capability of rapidly detecting, isolating and reconfiguring the AOCS minimizing the loss of performances, it can still be improved. The techniques presented cover the most common faulty cases, but a complete robustness has not been achieved yet. In addition, it is necessary to perform more tests to optimize the decision problem and avoid false alarms and non-detected faults.

The increment of the autonomy and probability of success, the optimization of resources and the reduction of critical situations encourage further research in FDIR systems.

5. Acknowledgements

This research was supported by Klepsydra Robotics in the frame of software development for space sector.

References

[1] D. Bock and M. Tajmar. Highly miniaturized feep propulsion system (nanofeep) for attitude and orbit control of cubesats. *Acta Astronautica*, (144):422–428, 2018.

[2] S. de Florio. Precise autonomous orbit control in low earth orbit: from design to flight validation. PhD thesis, University of Glasgow, May 2013.

DOI: 10.13009/EUCASS2019-702

[3] Duarte Otero de Morais Alves Rondao. Modeling and simulation of the ecosat-iii attitude determination and control system. Master's thesis, Tecnico Lisboa, April 2016.

[4] M. Eliasson. A kalman filter approach to reduce position error for pedestrian applications in areas of bad GPS reception. Degree project, Umea University, Spring 2014.

[5] R. Fonod. Diagnostique de defaut a base de modele et accommodation de defaut pour missions spatiales. PhD thesis, Universite de Bordeaux, November 2014.

[6] E. A. Hogan and H. Schaub. Three-axis attitude control using redundant reaction wheels with continuous momentum damping. *AAS/AIAA Spaceflight Mechanics Meeting*, 13(292), February 2013.

[7] Zuliana Ismail and Renuganth Varatharajoo. A study of reaction wheel configurations for a 3-axis satellite attitude control. *Advances in Space Research*, 45:750–759, 2010.

[8] Xavier Olive. Fdi(r) for satellites: How to deal with high availability and robustness in the space domain? *Int. J. Appl. Math. Comput. Sci.*, 22(1):99–107, 2012.

[9] M. J. Sidi. *Spacecraft Dynamics and Control: A Practical Engineering Approach*. Cambridge University Press, 1 edition, 1997.

[10] A. Tewari. *Modern Control Design with Matlab and Simulink*. John Wiley and Sons, 2002.

[11] Ali Zolghadri, David Henry, Jereme Cieslak, Denis Efimov, and Philippe Goupil. *Fault Diagnosis and Fault-Tolerant Control and Guidance for Aerospace Vehicles: From Theory to Application*. Advances in Industrial Control. Springer London, London, 2014 edition, 2014.